



# Enhanced High-Voltage Cycling Stability of Nickel-Rich Cathode Materials by Surface Modification Using $\text{LaFeO}_3$ Ionic Conductor

JUFENG ZHANG,<sup>1,2</sup> TING REN,<sup>1,2</sup> JIANGUO DUAN,<sup>1,2,3</sup>  
XUE LI,<sup>1,2</sup> PENG DONG,<sup>1,2</sup> YINGJIE ZHANG,<sup>1,2,4</sup> and  
DING WANG<sup>1,2,5</sup>

1.—National and Local Joint Engineering Laboratory for Lithium-ion Batteries and Materials Preparation Technology, Faculty of Metallurgical and Energy Engineering, Kunming University of Science and Technology, Kunming 650093, People's Republic of China. 2.—Key Laboratory of Advanced Battery Materials of Yunnan Province, Faculty of Metallurgical and Energy Engineering, Kunming University of Science and Technology, Kunming 650093, People's Republic of China. 3.—e-mail: duanjianguo@kmust.edu.cn. 4.—e-mail: zyjkmust@126.com. 5.—e-mail: wangdingliverpool@foxmail.com

$\text{LaFeO}_3$  is introduced as an ideal protective coating layer with excellent conductivity to enhance  $\text{LiNi}_{0.5}\text{Co}_{0.2}\text{Mn}_{0.3}\text{O}_2$  (NCM523) cathode material for use at higher operating voltage (especially 4.6 V). Various material characterization methods are employed to characterize the structural and morphological characteristics of the pristine and modified samples, including x-ray diffraction analysis, field-emission scanning electron microscopy, transmission electron microscopy, and x-ray photoelectron spectroscopy. The electrode with 2 wt.%  $\text{LaFeO}_3$  coating showed capacity retention of 80% at current density of 1 C after 200 charge/discharge cycles at 25°C, compared with 63% for the pristine electrode. Cyclic voltammogram results indicated that the  $\text{LaFeO}_3$  coating reduced the cell polarization during extended cycling. The results therefore show that  $\text{LaFeO}_3$  has potential for coating of NCM523 for use even at high voltage.

## INTRODUCTION

Over the last few decades, lithium ion batteries (LIBs) have become widespread, being used as power sources for many devices ranging from portable electronic devices to electric vehicles (EVs), as well as large-scale stationary energy storage systems. The resulting demand for LIBs with both high power density and high energy density has stimulated tremendous research effort to exploit high-performance electrode materials.  $\text{LiNi}_{0.5}\text{Co}_{0.2}\text{Mn}_{0.3}\text{O}_2$  (NCM523), a cathode material for LIBs, has attracted significant attention due to its high theoretical capacity and moderate cost.<sup>1–5</sup> Unfortunately, when such electrodes are charged at 4.6 V to achieve higher capacity, the NCM523 material often demonstrates poor cyclic stability, because the transition metals in the host structure may dissolve in the organic electrolyte and catalyze severe side-reactions at the interface.<sup>6–9</sup> HF and

LiF, i.e., organic and inorganic byproducts generated by the decomposition of the organic electrolyte, can also attach to the surface of the NCM523 cathode material, resulting in the appearance of a solid electrolyte interface (SEI) film that thickens as the charge–discharge cycles progress.<sup>10</sup> Owing to the poor electric and ionic conductivities of this SEI film, NCM523 cathodes exhibit fast capacity fading and poor rate capability.<sup>11</sup> Moreover, HF can result in erosion of the active material, thus degrading the cycling performance.<sup>12,13</sup> The performance degradation resulting from these failure mechanisms depends heavily on the surface state.<sup>14</sup>

Various strategies have been adopted to address these issues, including surface modification, elemental substitution, and electrolyte additives, among which surface coating has been demonstrated to represent a useful approach to enhance the structural stability and electrochemical performance, including cycling performance and rate

capability, of such cathode materials.<sup>15–21</sup> The coating materials typically used for such surface modification include metal oxides (e.g., CeO<sub>2</sub>, ZnO, and Y<sub>2</sub>O<sub>3</sub>), fluorides (e.g., AlF<sub>3</sub>), phosphates (e.g., LaPO<sub>4</sub>), and many inorganic materials (e.g., Li<sub>2</sub>ZrO<sub>3</sub>, Li<sub>2</sub>SiO<sub>3</sub>). Previous studies have indicated that such a surface coating can separate the cathode material from the electrolyte, thereby suppressing the side reaction caused by HF as well as the dissolution of transition metals.<sup>18–21</sup> Unfortunately, during the charge–discharge process, some of these inert materials may also hinder deintercalation of lithium ions.<sup>21</sup> Therefore, good candidate coating materials should exhibit the following properties: (1) high electrical/ionic conductivity to accelerate the transmission rate of Li<sup>+</sup>/electrons, and (2) good structural and thermal stability.<sup>20</sup>

Against this background, ABO<sub>3</sub>-type perovskite oxides have been adopted to coat the surface of NCM523 to enhance its electrochemical properties, due to their outstanding physical and chemical properties; For instance, some exhibit both high Li<sup>+</sup>/electron conductivity and good electrochemical stability because of their unique crystal structures.<sup>22</sup> LaFeO<sub>3</sub> perovskite is reported to be generally applicable for catalytic oxidation and in gas sensors, serving in particular as a surface coating material for electrodes in LIBs, based on its outstanding electrical and gas-sensitive characteristics.<sup>23</sup> In the bulk LaFeO<sub>3</sub> lattice, charge transfer is favored by the presence of oxygen vacancies, greatly enhancing its electrical conductivity.<sup>24</sup> It is clear that surface modification by coating with LaFeO<sub>3</sub> may be a useful approach to enhance the transmission rate of Li<sup>+</sup> and the electrical conductivity of NCM523 cathode material.<sup>23</sup> Furthermore, it may prevent corrosion by HF and maintain operation under extreme conditions such as high temperature. In addition, the interfacial stability of the cells may also be improved owing to the excellent structural stability of LaFeO<sub>3</sub>.

In this study, LaFeO<sub>3</sub> coating was used not only as a protective layer but also to act as an excellent Li<sup>+</sup> conductor. LaFeO<sub>3</sub>-modified NCM523 samples were prepared by a sol–gel method to obtain a uniform coating over the whole material. The cycle stability of the modified NCM523 was significantly enhanced with less capacity loss. In particular, the effects on the crystal structure, morphology, and electrochemical performance of NCM523 were systematically explored.

## EXPERIMENTAL PROCEDURES

### Preparation of LaFeO<sub>3</sub>-Coated NCM523

High-temperature solid-state sintering was used to prepare pristine NCM523 powder. First, commercial Ni<sub>0.5</sub>Co<sub>0.2</sub>Mn<sub>0.3</sub>(OH)<sub>2</sub> precursor was mixed with LiOH·H<sub>2</sub>O (99.9%, Aladdin) in a mortar at molar ratio of 1:1.05, and the mixture was ground for approximately 20 min, followed by sintering by a

two-step heating procedure in a muffle furnace, viz. precalcination at 500°C for 5 h and calcination at 900°C for 12 h. LaFeO<sub>3</sub>-coated NCM523 (denoted as LFO-*x*) was then synthesized by a sol–gel method. First, coating solution was prepared by dissolving La(NO<sub>3</sub>)<sub>3</sub>·6H<sub>2</sub>O (99.90%) particles and Fe(NO<sub>3</sub>)<sub>3</sub>·9H<sub>2</sub>O (98.50%) particles in absolute ethanol at molar ratio of 1:1. Subsequently, NCM523 powder was slowly dispersed into the coating solution described above under gentle magnetic stirring at 80°C, to evaporate the absolute ethanol. The resulting gels were dried in an oven at 80°C for 2 h to allow complete evaporation of the absolute ethanol, followed by sintering at 600°C for 2 h. The final sintered powders are denoted as LFO-0 (0 wt.% LaFeO<sub>3</sub> coating), LFO-1 (1 wt.% LaFeO<sub>3</sub> coating), LFO-2 (2 wt.% LaFeO<sub>3</sub> coating), and LFO-3 (3 wt.% LaFeO<sub>3</sub> coating).

### Material Characterization

The crystalline structure of the as-prepared samples was determined by x-ray diffraction (XRD) analysis using Cu K<sub>α</sub> radiation (Rigaku Mini-Flex600) in the 2θ range from 10° to 80° at scan rate of 2° min<sup>-1</sup> and room temperature. The micro-morphology of all the samples was investigated by field-emission scanning electron microscopy (FESEM, FEI Nova Nano SEM 450) and transmission electron microscopy (TEM, Hitachi, H-800, 200 kV). The surface state of the bare and modified samples was analyzed by x-ray photoelectron spectroscopy (XPS, Thermo ESCALAB250XI).

### Electrochemical Measurements

The cathode materials were used in CR-2025 coin cells to study their electrochemical performance. Further, 80 wt.% active material, 10 wt.% acetylene black as conductive agent, and 10 wt.% polyvinylidene fluoride (PVDF) as binder were mixed and ground for approximately 15 min in an agate mortar, and ground continually with dropwise addition of *N*-methylpyrrolidinone (NMP) into the mixture. After wet grinding for approximately 5 min, a homogenous slurry was obtained. Subsequently, the obtained slurry was coated evenly on Al foil. Subsequently, a heating process to dry the samples was performed at 120°C for 12 h under vacuum. Subsequently, CR-2025 cells was assembled in an Ar-filled glovebox using lithium metal sheet as anode and Celgard 2400 as separator. Ethylene carbonate (EC) and dimethyl carbonate (DMC) were mixed at volume ratio of 1:1 followed by addition of 1 M LiPF<sub>6</sub> to prepare the electrolyte. A LANHE battery test system (CT-2001A, China) was used to test the cycle performance of the coin cells in the voltage range from 3.0 V to 4.6 V (versus Li/Li<sup>+</sup>). Cyclic voltammetry (CV, scan rate 0.1 mV s<sup>-1</sup>, potential range 3.0 V to 4.6 V) and electrochemical impedance spectroscopy (EIS) were conducted using an electrochemical workstation (CHI660E, China).

## RESULTS AND DISCUSSION

### Physical Characterization

Figure 1 shows the XRD patterns of the LFO- $x$  ( $x = 0, 1, 2, 3$ ) samples. All peaks correspond to the layered hexagonal structure of  $\alpha$ -NaFeO<sub>2</sub> in space group  $R\bar{3}m$ . The sharp and well-defined peaks observed for all samples confirm that the LaFeO<sub>3</sub> coating had no significant effect on the host material. No impurity peaks indexed to LaFeO<sub>3</sub> were observed in the XRD patterns of the LFO-1 sample, likely owing to the low coating content. However, for the other LFO- $x$  ( $x = 2, 3$ ) samples, a weak diffraction peak for LaFeO<sub>3</sub> appeared at  $2\theta = 32.5^\circ$ , corresponding to Joint Committee on Powder Diffraction Standards (JCPDS) card no. 75-0439,<sup>24</sup> indicating successful formation of LaFeO<sub>3</sub>. Rietveld refinement was applied to further understand the effect of LaFeO<sub>3</sub> on the structural parameters of the cathode material.

Rietveld refinement results for the slowly scanned powder XRD profiles of the LFO-0 and LFO-2 samples are shown in Fig. 1b and c, respectively. The corresponding lattice parameters are listed in Table S-1 (Online Supplementary Material). The observed and calculated profiles match well, with low values of both  $R_{wp}$  and  $R_p$ , indicating accurate refinement results. All the lattice parameters for the two samples are close; in particular, the cation mixing degrees are almost the same. This indicates that the LaFeO<sub>3</sub> coating lies on the surface of NCM523, rather than entering the host material.

The SEM images in Fig. 2 show no distinct differences in the size range among all the samples with average particle diameter of approximately 12  $\mu\text{m}$  to 15  $\mu\text{m}$ . The surface of the LFO-0 particles (Fig. 2a and b) showed smooth and clear edges,

while the LaFeO<sub>3</sub>-coated NCM523 samples exhibited rough surface morphology. When a coating of 2 wt.% or 3 wt.% was applied, a homogeneous coating composed of island-like material formed on the surface of the LFO-2 (Fig. 2c and g) and LFO-3 samples (Fig. 2d and h). Owing to the thicker and denser coating layer, the interstices between the primary particles were blurred and could barely be distinguished. Figure S-1 (Online Supplementary Material) shows energy-dispersive x-ray spectroscopy (EDS) mapping images of the LFO-2 sample. A uniform distribution of transition-metal elements such as Ni, Co, and Mn is observed in the LFO-2 sample. As expected, the La and Fe elements from the LaFeO<sub>3</sub> coating exhibited the same distribution range as the abovementioned three elements, indicating that the surface of the NCM523 powder was uniformly wrapped with a LaFeO<sub>3</sub> layer (Fig. S-1b–f).

Figure S-2 (Online Supplementary Material) shows high-resolution (HR)TEM images of the LFO-0 and LFO-2 samples. No material was detected on the surface of the pristine NCM523 (Fig. S-2a), consistent with the SEM results (Fig. 2a). In contrast to the bare sample, the surface of the LFO-2 sample (Fig. S-2b) was wrapped with some small particles. The measured lattice spacing of the coating layer was approximately 0.29 nm (Fig. S-2c), in agreement with the (110) planes of LaFeO<sub>3</sub>, confirming successful formation of the LaFeO<sub>3</sub> coating layer.<sup>24</sup> A uniform LaFeO<sub>3</sub> layer can act as a physical barrier to avoid unwanted reactions between the active material and organic electrolyte.

Figure S-3 (Online Supplementary Material) shows the XPS survey spectrum of the LFO-0 and LFO-2 samples, confirming the presence of transition-metal elements (Ni, Co, and Mn) as well as La

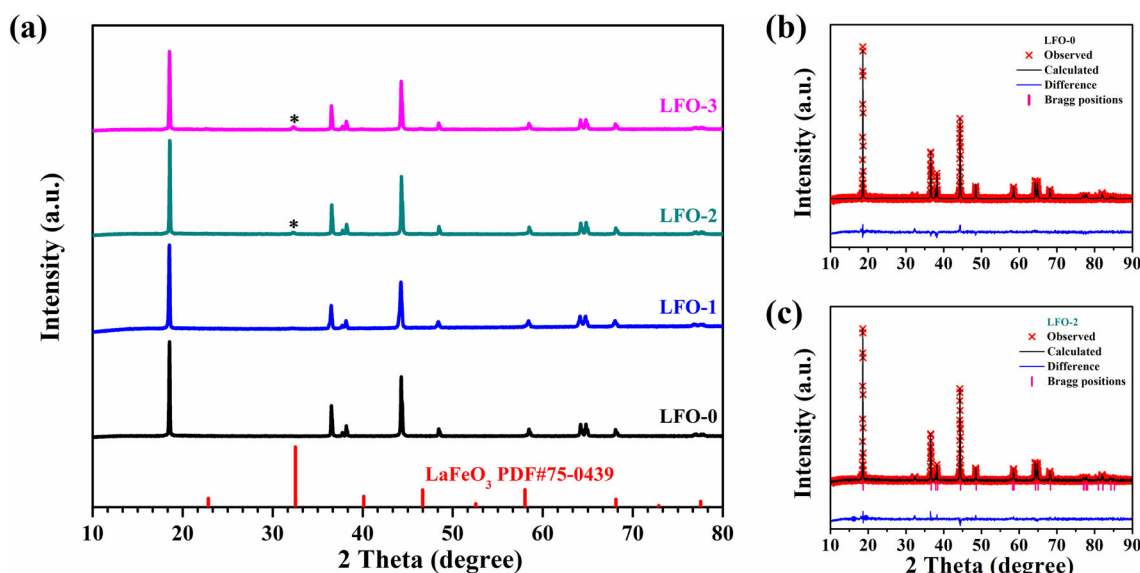


Fig. 1. (a) XRD patterns of the LFO- $x$  samples, and Rietveld refinement results for the (b) LFO-0 and (c) LFO-2 samples.

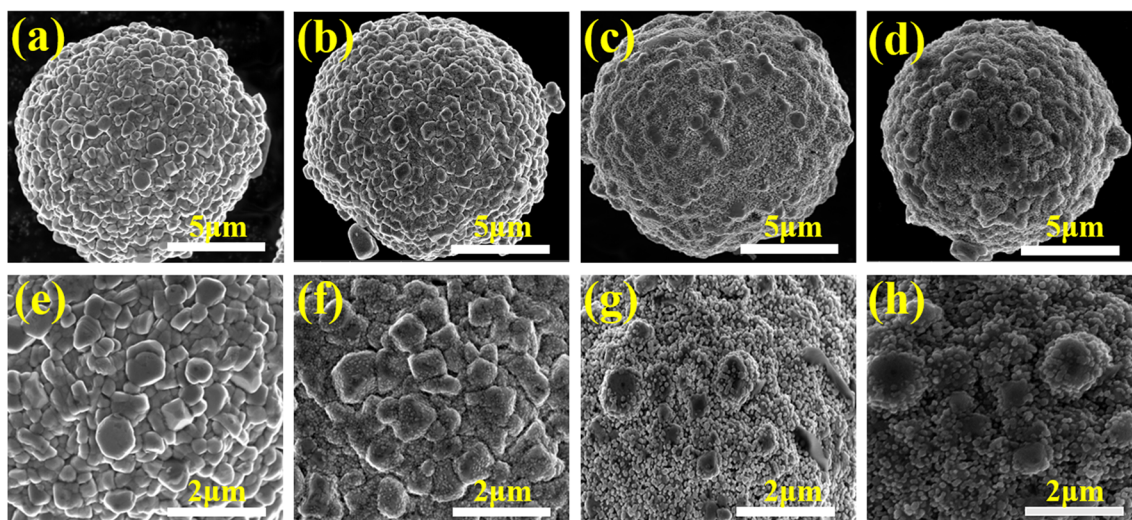


Fig. 2. SEM images of LFO-0 (a, e), LFO-1 (b, f), LFO-2 (c, g), and LFO-3 (d, h).

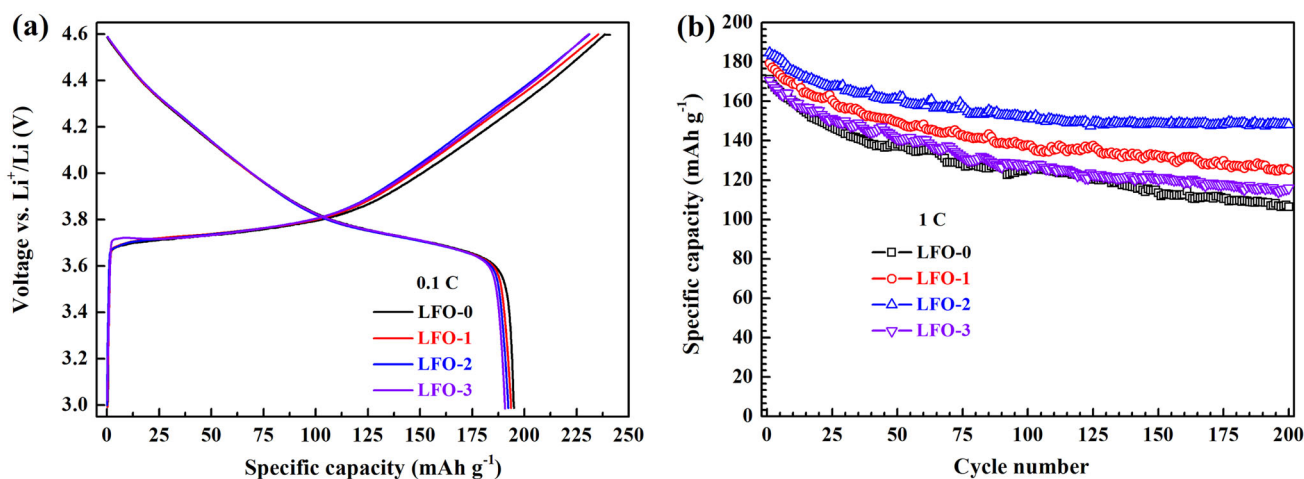


Fig. 3. (a) Initial charge–discharge curves at 0.1 C, (b) cyclic performance at 1 C for LFO- $x$  ( $x = 0, 1, 2, 3$ ) electrodes. 1 C = 180 mA g<sup>-1</sup>, 3.0 V to 4.6 V.

and Fe. The binding energy positions of the Ni 2*p*, Co 2*p*, and Mn 2*p* signals did not change significantly for either LFO- $x$  sample, having values of 854.6 eV, 778.2 eV, and 642.4 eV, respectively (Fig. S-3b–d). In particular, as shown in Fig. S-3e, both the La 3*d*<sub>3/2</sub> and La 3*d*<sub>5/2</sub> peaks showed a distinct splitting, resulting in four La 3*d* signals located at 861.4 eV, 853.9 eV, 837.8 eV, and 834.4 eV. The Fe 2*p* peak in Fig. S-3f is split into 2*p*<sub>3/2</sub> near 711.6 eV and 2*p*<sub>1/2</sub> near 724.8 eV, suggesting the presence of Fe as Fe<sup>2+</sup> in LaFeO<sub>3</sub>.<sup>25</sup> Comparison with standard data therefore confirms the formation of LaFeO<sub>3</sub> on the surface of NCM523.

### Electrochemical Performance

Figure 3 shows the initial charge–discharge curves of the LFO- $x$  electrodes at 0.1 C (1 C = 180 mA g<sup>-1</sup>) between 3.0 V and 4.6 V. The curves of all the samples exhibit a plateau starting

at 3.75 V, which is due to gradual oxidation of the nickel ion from a lower to higher valence state. The initial discharge capacity of the LFO-0 electrode was 195 mAh g<sup>-1</sup> (Fig. 3a), higher than those of the LaFeO<sub>3</sub>-coated electrodes: 193.5 mAh g<sup>-1</sup> for LFO-1, 192 mAh g<sup>-1</sup> for LFO-2, and 191.7 mAh g<sup>-1</sup> for LFO-3. This is because the LaFeO<sub>3</sub> phase is electrochemically inactive.

All the cells were initially charged/discharged at 0.1 C, 0.2 C, and 0.5 C thrice, and subsequently 200 times at 1 C in the voltage range of 3.0 V to 4.6 V. As shown in Fig. 3b, the electrodes coated with small amounts of LaFeO<sub>3</sub> exhibited superior lithium storage ability compared with the bare LFO-0 electrode over 200 cycles at room temperature. The initial discharge capacity of LFO-0 was 171 mAh g<sup>-1</sup>, which reduced to 107 mAh g<sup>-1</sup> after 200 cycles with capacity retention of 63%. Compared with the LFO-0 electrode, the LFO- $x$  ( $x = 1, 2,$

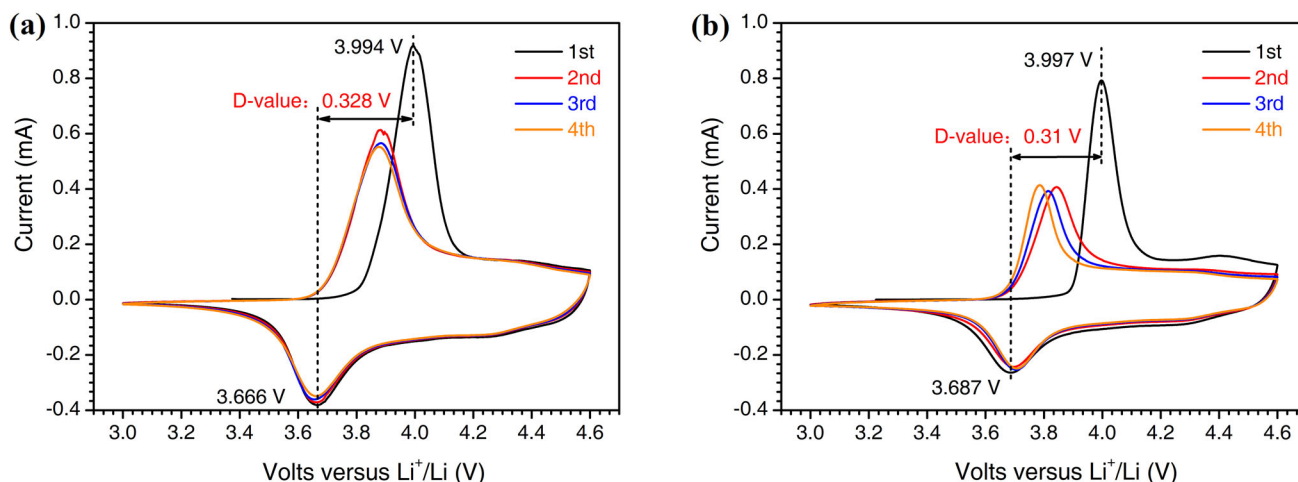


Fig. 4. CV curves for (a) LFO-0 and (b) LFO-2 electrodes between 3.0 V and 4.6 V with scan rate of 0.1 mV s<sup>-1</sup>.

3) electrodes delivered higher discharge capacities of 125 mAh g<sup>-1</sup>, 148 mAh g<sup>-1</sup>, and 116 mAh g<sup>-1</sup> after 200 cycles, respectively. All the LaFeO<sub>3</sub>-coated electrodes exhibited better cycling durability than LFO-0, viz. 70% for LFO-1, 80% for LFO-2, and 68% for LFO-3. This enhancement can be attributed to the change in the surface chemistry. Coating with a moderate amount of LaFeO<sub>3</sub> not only provided anticorrosion protection of the NCM523 surface but also accelerated diffusion of lithium ions.

Figure S-4 (Online Supplementary Material) shows the Nyquist plots of the LFO-0 and LFO-2 electrodes in the fully charged state. In general, the semicircle in the high-frequency range is attributed to the impedance of the solid electrolyte interface (SEI) layer ( $R_{sei}$ ) formed on the electrode surface, whereas the semicircle in the intermediate-frequency region is related to the interfacial charge transfer resistance ( $R_{ct}$ ), and the low-frequency oblique line corresponds to the Warburg impedance ( $W$ ).<sup>26,27</sup> The lithium ion diffusion coefficient ( $D_{Li^+}$ ) was obtained using a formula in Ref. <sup>28</sup>. The fit resistance values and  $D_{Li^+}$  values are listed in Table S-2. The LFO-0 electrode showed a higher  $R_{sei}$  value compared with the LFO-2 electrode after 10 and 50 cycles, indicating that LFO-2 possessed a more stable surface. Moreover, the  $R_{ct}$  value of the LFO-0 electrode was 175.6 Ω after 10 cycles, increasing to 325.5 Ω after 50 cycles. In comparison, the  $R_{ct}$  value of the LFO-2 electrode was 80.5 Ω after 10 cycles, increasing slowly to 123.6 Ω after 50 cycles, with a  $D_{Li^+}$  value of  $5.13 \times 10^{-11}$  cm<sup>2</sup> s<sup>-1</sup> after 10 cycles. The lithium ion diffusion rate in the LFO-2 electrode was higher than that in the LFO-0 electrode ( $1.16 \times 10^{-11}$  cm<sup>2</sup> s<sup>-1</sup>). The stable resistance and faster lithium ion diffusion rate found for the LFO-2 electrode can be attributed to suppression of the interfacial side reactions and the superior lithium ion transport ability conferred by the LaFeO<sub>3</sub> coating.

Figure 4 shows the CV results for the first four cycles of LFO-0 and LFO-2. The redox peak of the two electrodes displays a similar shape, indicating that the LaFeO<sub>3</sub> coating layer did not participate in the electrochemical reaction during the lithiation/delithiation process. The difference in the redox potential ( $D$ -value) of the LFO-2 electrode (0.31 V) was smaller than that of LFO-0 for the first cycle (0.328 V). Moreover, the  $D$ -values of the following cycles for the LFO-2 electrode were also lower than those of LFO-0. Therefore, the LaFeO<sub>3</sub> coating could improve the reversibility and reactivity of the NCM523 electrode even under high voltages.

Figure S-5 shows the morphologies of LFO-0 and LFO-2 after 200 cycles at 1 C. As shown in these two images, the particles of the LFO-0 sample split into small fragments. In accordance with the cyclic durability data in Fig. 3b, such pulverization of the LFO-0 electrode could cause rapid deterioration in its electrochemical performance. Compared with the morphology of the LFO-0 sample, LFO-2 retained a spherical shape after repeated cycles (Fig. S-5b), demonstrating that the LaFeO<sub>3</sub> coating persistently protected the active material from acid corrosion by the organic electrolyte, resulting in the enhanced high-voltage cycling properties of the modified NCM523 electrode materials.

## CONCLUSION

A uniform LaFeO<sub>3</sub> coating layer was formed on NCM523 layered oxide using a facile and efficient sol-gel method. No change in the crystalline structure of the host was observed after LaFeO<sub>3</sub> modification. The coating not only served as a protective layer for the host material, but also favored transportation of lithium ions through the interface. Although the initial discharge capacity of the modified electrodes at 0.1 C indicated a slight decline compared with the pristine electrode, the cyclic durability of the coated electrodes was significantly

enhanced. These findings indicate that  $\text{LaFeO}_3$  could serve as a reliable coating material to improve the cycle performance under high voltages.

### ACKNOWLEDGEMENTS

The authors acknowledge financial support from the National Science Foundation of China (51804149, 51764029), Provincial Natural Science Foundation of Yunnan (2018FD039), and National Key R&D Program of China (2018YFB0104000).

### ELECTRONIC SUPPLEMENTARY MATERIAL

The online version of this article (<https://doi.org/10.1007/s11837-019-03446-3>) contains supplementary material, which is available to authorized users.

### REFERENCES

- J.M. Tarascon and M. Armand, *Nature* 414, 359 (2001).
- W. Liu, P. Oh, X. Liu, M.J. Lee, W. Cho, S. Chae, Y. Kim, and J. Cho, *Angew. Chem. Int. Ed.* 54, 4440 (2015).
- P. Dong, D. Wang, Y. Yao, X. Li, Y. Zhang, J. Ru, and T. Ren, *J. Power Sources* 344, 111 (2017).
- J.B. Goodenough and Y. Kim, *Chem. Mater.* 22, 587 (2010).
- K.P. Wu, K. Du, and G.R. Hu, *J. Mater. Chem. A* 6, 1057 (2018).
- S.K. Jung, H. Gwon, J. Hong, K.Y. Park, D.H. Seo, H. Kim, J. Hyun, W. Yang, and K. Kang, *Adv. Energy Mater.* 4, 1300787 (2014).
- M. Noh and J. Cho, *J. Electrochem. Soc.* 160, A105 (2012).
- K.P. Wu, K. Du, and G.R. Hu, *J. Mater. Chem. A* 6, 3444 (2018).
- K.P. Wu, D. Liu, and Y. Tang, *Electrochim. Acta* 263, 515 (2018).
- Y.K. Sun, S.T. Myung, B.C. Park, J. Prakash, I. Belharouak, and K. Amine, *Nat. Mater.* 8, 320 (2009).
- F. Wu, J. Tian, Y. Su, Y. Guan, Y. Jin, Z. Wang, T. He, L. Bao, and S. Chen, *J. Power Sources* 269, 747 (2014).
- H. Zhu, T. Xie, Z. Chen, L. Li, M. Xu, W. Wang, Y. Lai, and J. Li, *Electrochim. Acta* 135, 77 (2014).
- D. Wang, Z. Wang, X. Li, H. Guo, Y. Xu, Y. Fan, and W. Pan, *Appl. Surf. Sci.* 371, 172 (2016).
- D. Wang, X. Li, Z. Wang, H. Guo, Y. Xu, Y. Fan, and J. Ru, *Electrochim. Acta* 188, 48 (2016).
- K. Liu, G.L. Yang, Y. Dong, T. Shi, and L. Chen, *J. Power Sources* 281, 370 (2015).
- J.Z. Kong, C. Ren, G.A. Tai, X. Zhang, A.D. Li, D. Wu, H. Li, and F. Zhou, *J. Power Sources* 266, 433 (2014).
- X.H. Liu, L.Q. Kou, T. Shi, K. Liu, and L. Chen, *J. Power Sources* 267, 874 (2014).
- K. Yang, L. Fan, J. Guo, and X. Qu, *Electrochim. Acta* 63, 363 (2012).
- H.G. Song, K.-S. Park, and Y.J. Park, *Solid State Ion.* 225, 532 (2012).
- D. Wang, X. Li, Z. Wang, H. Guo, Z. Huang, L. Kong, and J. Ru, *J. Alloys Compd.* 647, 612 (2015).
- D. Wang, X. Li, Z. Wang, H. Guo, X. Chen, X. Zheng, Y. Xu, and J. Ru, *Electrochim. Acta* 174, 1225 (2015).
- Y. Shao-Horn, *Nat. Chem.* 3, 546 (2011).
- P. Ciambelli, S. Cimino, R.S. De, L. Lisi, G. Minelli, P. Porta, and G. Russo, *Appl. Catal.* 29, 239 (2001).
- P.V. Gosavi and R.B. Biniwale, *Mater. Chem. Phys.* 119, 324 (2010).
- J. Mou, Y. Deng, L. He, Q. Zheng, N. Jiang, and D. Lin, *Electrochim. Acta* 260, 101 (2018).
- Q. Ye, J. Ru, J. Peng, G. Chen, and D. Wang, *Chem. Eng. J.* 331, 570 (2018).
- J.W. Kim, D.H. Kim, D.Y. Oh, H. Lee, J.H. Kim, J.H. Lee, and Y.S. Jung, *J. Power Sources* 274, 1254 (2015).
- C. Ho, I.D. Raistrick, and R.A. Huggins, *J. Electrochem. Soc.* 127, 343 (1980).

**Publisher's Note** Springer Nature remains neutral with regard to jurisdictional claims in published maps and institutional affiliations.